Longitudinal map of transcriptome changes in the Lyme pathogen *Borrelia burgdorferi* during tick-borne transmission

Anne L. Sapiro[1*], Beth M. Hayes[1], Regan F. Volk[2], Jenny Y. Zhang[1], Diane M. Brooks[3], Calla Martyn[1], Atanas Radkov[1], Ziyi Zhao[1], Margie Kinnersley[3], Patrick R. Secor[3], Balyn W. Zaro[2], Seemay Chou[1*]

1 Department of Biochemistry & Biophysics, University of California, San Francisco, California, USA
2 Department of Pharmaceutical Chemistry and Cardiovascular Research Institute, University of California, San Francisco, California, USA
3 Division of Biological Sciences, University of Montana, Missoula, Montana, USA

*Corresponding authors:
Anne L. Sapiro: annesapiro@gmail.com & Seemay Chou: seemaychou@gmail.com

ABSTRACT

Borrelia burgdorferi (*Bb*), the causative agent of Lyme disease, must adapt to vastly different environments as the bacterium cycles between the tick vector and a vertebrate host. During a bloodmeal, *Bb* migrates from the tick midgut to the salivary glands and changes its gene expression, priming *Bb* for vertebrate infection. These tick-specific transmission events are dependent on key transcriptional regulators; however, the full range of transcriptional changes that occur over several days inside of the tick are technically challenging to capture. We developed an experimental approach to enrich *Bb* cells from *Ixodes* ticks during a transmitting bloodmeal to longitudinally define their global transcriptomic landscape. We identified 192 genes that substantially change expression over the course of the tick bloodmeal, most of which were located on plasmids of the *Bb* genome. The majority of upregulated genes encode proteins found at the cell envelope or proteins of unknown function, including 45 outer surface lipoproteins embedded in the unusual protein-rich coat of *Bb*. As these proteins may facilitate *Bb* interactions with host tissues or immune systems, we also utilized mass spectrometry to identify candidate tick proteins that physically associate with *Bb*. The *ex vivo Bb* transcriptomes and candidate tick interacting proteins presented here provide an important roadmap for investigating key determinants of *Bb* priming and transmission during the tick stage of its unique transmission cycle.

INTRODUCTION

Vector-borne microbial pathogens are transmitted by the bite of arthropods and have evolved sophisticated ways to adapt to vastly different environments as they move between vector and host. Uncovering their adaptive mechanisms can not only open avenues for disrupting pathogen transmission but also provide fundamental insights into vector physiology and microbial symbioses (Shaw and Catteruccia, 2018). Lyme disease, the most reported vector-borne disease in North America, is caused by the bacterial pathogen *Borrelia burgdorferi* (*Bb*) (Rosenberg et al., 2018; Steere et al., 2016). Its primary vector, the blacklegged tick *Ixodes scapularis,* acquires and transmits *Bb* through two separate multi-day bloodmeals, one in which *Bb* is acquired from an infected vertebrate host and a second, during the subsequent life stage, in which *Bb* is transmitted to a new host (Tilly et al., 2008). During the transmission bloodmeal, *Bb* proliferate in the tick midgut before a subset of these cells disseminate to the salivary glands (Dunham-Ems et al., 2009). *Bb* is deposited into the new host via the tick saliva extruded into the bite site (Spielman et al., 1987). Given the prolonged nature of *I. scapularis* feeding, the high specificity of vector-pathogen relationships, and the complicated array of events needed for successful *Bb* transmission, the tick bloodmeal provides an opportune intervention point for preventing pathogen spread. However, we do not currently have a clear understanding of the molecular mechanisms involved in this process.

Bb must adapt to dramatically different environments as it cycles from tick to vertebrate host, and understanding the genes involved in this process will enable the identification of key interactions to target to prevent transmission. When an infected tick feeds, *Bb* responds to bloodmeal-induced environmental changes and undergoes cellular modifications driven by key transcriptional circuits, including the RpoN-RpoS sigma factor cascade and the Hk1/Rrp1 two-component system (Radolf et al., 2012). *In vitro* analyses of *Bb* cells cultured in tick- or mammalian-like growth conditions have pointed to additional genetic determinants of tick-borne transmission by revealing widespread transcriptome remodeling during host switching (reviewed in Samuels et al., 2021). However, it is not fully clear how these *in vitro* expression changes correspond to complex *in vivo* changes over the course of a transmission bloodmeal, which comprises several physiologically distinct stages for the tick vector. Capturing comprehensive, longitudinal data on *Bb* expression from inside its vector has been hampered by technical challenges given the dynamic nature of the bloodmeal and the general low abundance of bacterial cells relative to the tick (Samuels et al., 2021). Although microarray approaches have been used to identify large scale changes in *Bb* gene expression between the first and second tick bloodmeals (Iyer et al., 2015), we have limited

69 temporal resolution into the molecular transitions that happen across key steps of tick feeding.
70 This problem necessitates novel approaches to capture the transcriptomic changes of *Bb* within
71 the natural tick environment.
72
73 While the full landscape of *Bb* transmission determinants is not yet known, we do have a growing
74 knowledge of functional processes that are critical during the tick stage, such as motility,
75 metabolism, and immune evasion (Kurokawa et al., 2020; Phelan et al., 2019). These functions
76 often rely on the unique protein-rich *Bb* outer surface. Notably, several specific tick–*Bb* protein–
77 protein interactions are important for *Bb* survival, migration, or transmission to the next host. *Bb*
78 encodes an extensive outer surface protein (Osp) family with members that are differentially
79 expressed during host switching. One of these proteins, OspA, binds a tick cell surface protein,
80 tick receptor for OspA (TROSPA), which is required for successful *Bb* colonization of the tick
81 midgut during the first acquisition bloodmeal (Pal et al., 2004). Several other proteins have also
82 been linked to *Bb* migration within the tick (Pal et al., 2022). For example, BBE31 binds a tick
83 protein TRE31, and disruption of this interaction decreases the number of *Bb* cells that
84 successfully migrate from the tick gut to salivary glands (Zhang et al., 2011). However, these
85 interactions alone are not sufficient to block *Bb* growth or migration in ticks, suggesting there are
86 likely additional molecular factors from *Bb* and ticks at play during tick-borne transmission.
87
88 To provide a more comprehensive set of *Bb* determinants driving tick-borne transmission of this
89 important human pathogen, we longitudinally mapped *Bb* genome-wide expression changes for
90 bacterial cells isolated from inside ticks during the transmission bloodmeal. We developed a novel
91 sequencing-based strategy for *ex vivo* transcriptomic profiling of *Bb* populations within feeding
92 ticks. We identified 192 highly differentially expressed genes, including both genes previously
93 implicated in *Bb* transmission as well as many others. Genes upregulated during tick transmission
94 were enriched for outer surface lipoproteins, suggesting *Bb* dramatically remodels its cell
95 envelope as it migrates through the tick. Mass spectrometry analyses revealed dramatic changes
96 in the tick environment over feeding, identifying new potential determinants of a more extensive
97 and diverse set of tick–microbe molecular interactions than previously appreciated.
98
99 **RESULTS**
100 **A two-step enrichment process facilitates robust transcriptional profiling of *Bb* during the**
101 **tick bloodmeal**
102

To gain a more comprehensive understanding of *Bb* gene expression throughout the tick phase of the transmission cycle, we developed an experimental approach to characterize the *Bb* transcriptome of spirochetes isolated from ticks during a bloodmeal. We aimed to establish a longitudinal transcriptional profile encompassing key pathogen transmission events each day of feeding after ticks attached to their mouse bloodmeal hosts (**Figure 1A**). The major bottleneck for such an RNA sequencing (RNA-seq) approach is capturing sufficient quantities of *Bb* transcripts from complex multi-organism samples in which pathogen transcripts represent a very small minority. Our initial attempts to uncover *Bb* mRNA by simply removing tick mRNA with polyA-depletion and removing tick rRNA sequences using Depletion of Abundant Sequences by Hybridization (DASH) (Dynerman et al., 2020; Gu et al., 2016) were unsuccessful. This approach resulted in an average of only 0.09% of RNA-seq reads mapping to *Bb* mRNA – approximately 10-fold less than we estimated would be needed to feasibly obtain robust transcriptome-wide gene expression analysis (Haas et al., 2012).

To dramatically increase *Bb* transcript representation in our libraries, we physically enriched *Bb* cells in tick lysates prior to library preparation by adding an initial step of immunomagnetic separation (**Figure 1B**). We took advantage of a commercial antibody previously generated against whole *Bb* cells (α*Bb*, RRID: AB_1016668). By western blot analysis, we confirmed that α*Bb* specifically recognized several *Bb* proteins, including surface protein OspA, which is highly prevalent on the *Bb* surface in ticks (**Figure S1A**). In addition, immunofluorescence microscopy with α*Bb* showed clear recognition of *Bb* cells from within the tick at each day of feeding (**Figure S1B**). After collecting infected ticks from mice one, two, three, and four days post-attachment, we used α*Bb* and magnetic beads to enrich *Bb* cells away from the majority of the tick material in the lysates. We tracked relative *Bb* enrichment through RT-qPCR of *Bb flaB* RNA and tick *gapdh* RNA in the separated samples. Measuring *Bb flaB* RNA from both *Bb*-enriched samples and their

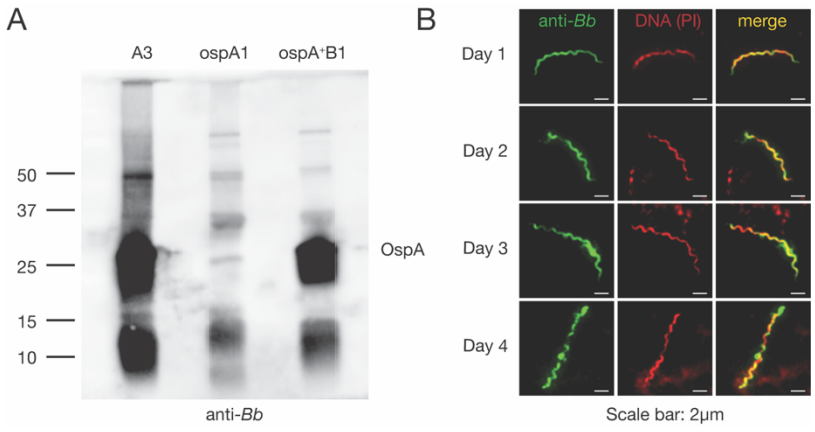

Figure S1. Anti-*Bb* antibody recognizes ospA and binds *Bb* in the tick throughout the bloodmeal. (**A**) Western blot with anti-*Bb* on lysate from cultured *Bb*: wildtype (A3, left), a mutant lacking ospA (ospA1), and the mutant with ospA restored (ospA+B1). Anti-*Bb* recognizes ospA among other proteins. (**B**) Immunofluorescence microscopy with anti-*Bb* (green) and propidium iodide (PI) (DNA, red) on each day of feeding (yellow is merge). Anti-*Bb* antibody recognizes *Bb* in the tick across the bloodmeal.

matched *Bb*-depleted fractions, we found over 95% of total *Bb flaB* RNA was present in enriched fractions (**Figure 1C**), suggesting our approach captured the vast majority of *Bb* transcripts from the tick.

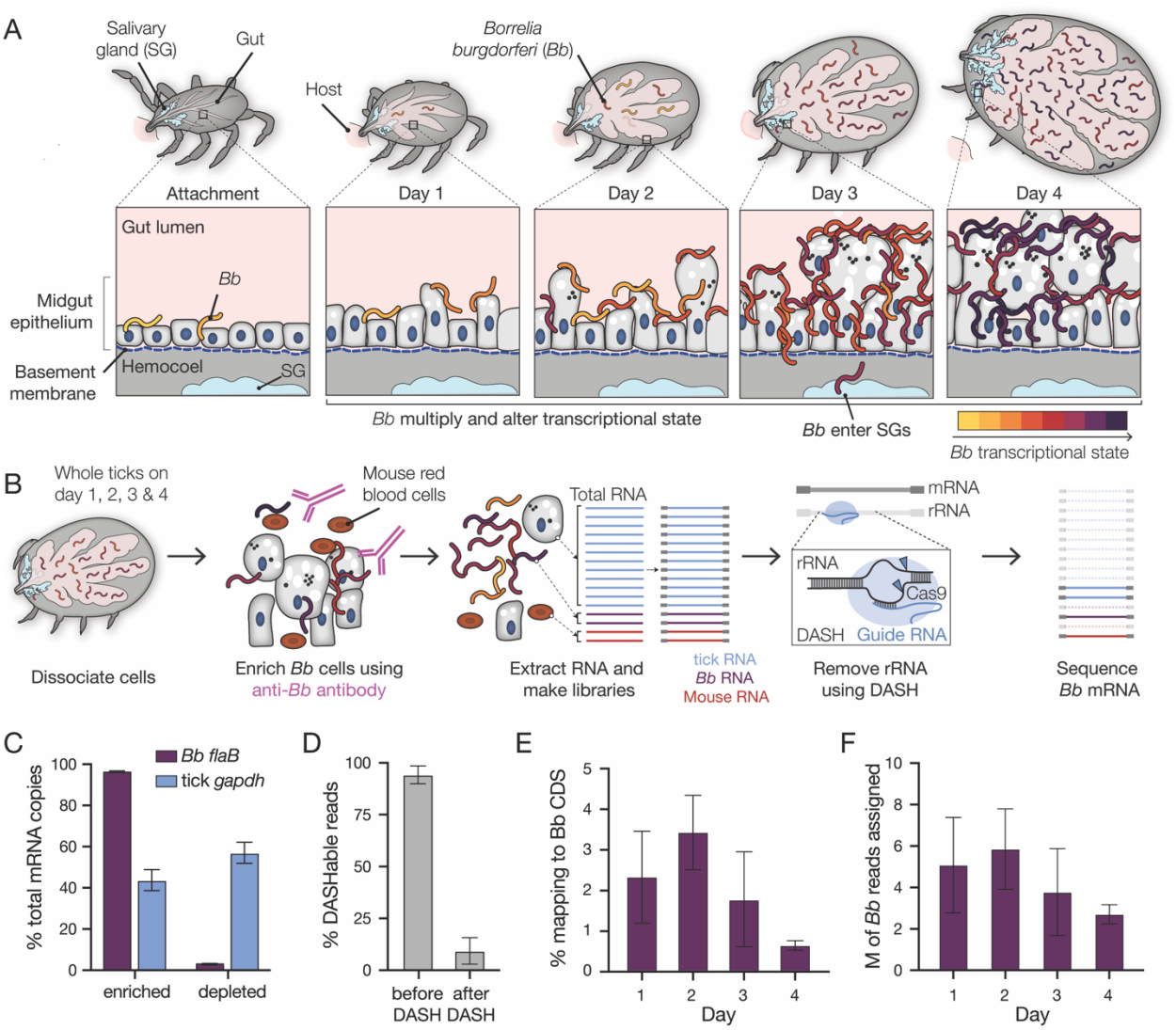

Figure 1. A two-step enrichment process facilitates robust transcriptional profiling of *Bb* during the tick bloodmeal. (**A**) Schematic of *Bb* during tick feeding. *Bb* in the nymphal tick midgut respond to the bloodmeal by multiplying and changing their transcriptional state. At the same time, the tick gut undergoes numerous changes to digest the bloodmeal. After two to three days of feeding, a small number of *Bb* leave the midgut and enter the salivary glands (blue), while the majority are left behind in the gut after engorgement. (**B**) Schematic of *Bb* enrichment process from feeding ticks. Whole ticks are dissociated, anti-*Bb* antibodies are added to lysates, and antibodies and *Bb* are captured magnetically. RNA is extracted and RNA-seq libraries are prepared. DASH is then used to remove rRNA before sequencing. This process increases *Bb* reads in the resulting sequencing. (**C**) RT-qPCR results showing the percentage of *Bb flaB* and tick *gapdh* RNA in the enriched versus depleted fractions after the enrichment process. Data come from 4 replicates each from day 2, day 3, and day 4, mean +/- SE. Nearly all *Bb flaB* RNA was found in the enriched fraction, while the majority of tick *gapdh* was found in the depleted fraction. (**D**) The percentage of reads mapping to rRNA before and after DASH. Data are shown as mean +/- SD. rRNA reads are drastically reduced after DASH. (**E**) The percentage of reads in RNA-seq libraries mapping to *Bb*. *Bb* mRNA reads make up a small but sufficient proportion of libraries for transcriptomics. Data are shown as mean +/- SD. (**F**) The number of reads in millions (M) mapped to *Bb* for each day. Data are shown as mean +/- SD. An average of 4.3 million reads per sample mapped to Bb genes, covering 92% of genes with at least 10 reads.

Total RNA recovered from the enrichment process was used to create RNA-seq libraries that subsequently underwent depletion of rRNA sequences from ticks, mouse, and *Bb* using DASH, which targets unwanted sequences for degradation by Cas9 (Gu et al., 2016; Ring et al., 2022). DASH reduced unwanted sequences from 94% to 9% of our total libraries, greatly increasing the relative abundance of *Bb* transcripts (**Figure 1D**). For resulting libraries generated across feeding (**Table S1**), between 0.6% and 3.4% of reads mapped to *Bb* coding regions (**Figure 1E**), which translated to an average of 4.3 million *Bb* reads per sample (**Figure 1F**). Read coverage was sufficient for downstream differential expression analyses for the vast majority of *Bb* genes, with at least 10 reads mapping to 92% of *Bb* genes. To evaluate whether our approach introduced any major artifacts, we sequenced and compared RNA-seq libraries from *in vitro* cultured *Bb* cells before and after immunomagnetic enrichment. We found minimal expression differences (29 genes with p<0.05, fold changes between 0.83-1.12) (**Figure S2, Table S2**), suggesting experimental enrichment did not significantly alter global transcriptome profiles for *Bb*. Thus, we developed an approach to enable genome-wide analysis of *Bb* population-level expression changes that occur within the feeding tick during transmission.

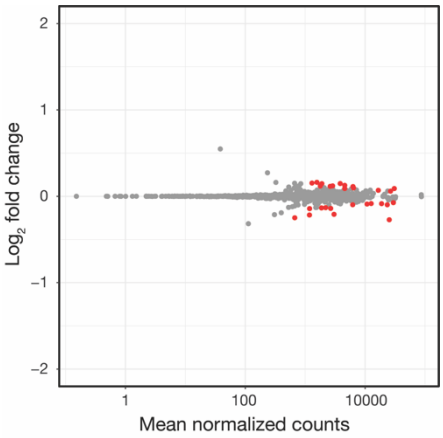

Figure S2. Enrichment process does not induce large scale gene expression changes in *in vitro* cultured *Bb*. Log_2 fold changes vs. mean normalized number of counts comparing cultured *Bb* input and samples after enrichment with anti-*Bb*. n=3. Red dots, p-value < 0.05, Wald tests. The gene expression changes induced during processing are much smaller than those observed between days of feeding.

Global *ex vivo* profiling of *Bb* reveals extent and kinetics of transcriptional changes

To provide a broad overview of *Bb* expression changes during feeding, we performed principal component analysis (PCA) on the *Bb* transcriptome data from one, two, three, and four days post-attachment (n=4). We reasoned that if many longitudinal expression changes were occurring across *Bb* populations, we would observe greater data variability between time points than between biological replicates. Indeed, we found replicates from each day grouped together, whereas distinct time points were largely non-overlapping. The first principal component, which explained 64% of the variance in our data, correlated well with day of feeding (**Figure 2A**). The global pattern suggested that *Bb* gene expression changes generally trended in the same

direction over the course of feeding with the most dramatic differences between flanking timepoints on day 1 and day 4.

Using day 1 (early attachment) as a baseline, we performed differential expression analysis for all *Bb* genes at subsequent time points and examined changes above a twofold threshold (**Figure 2B, Table S3**). These analyses mirrored the global longitudinal expression pattern predicted by our PCA. The total number of differentially expressed (DE) genes increased steadily over time and peaked at day 4, which when compared to day 1 had 186 DE genes, including 153 upregulated and 33 downregulated (**Figure 2C-E**). Across time points, DE genes were highly overlapping and largely changed in the same directions. In all three comparisons, we found 192 DE genes in total (**Table S4**). However, there were some notable differences between genes, such as the overall timing and kinetics of expression changes. Transcript levels for some DE

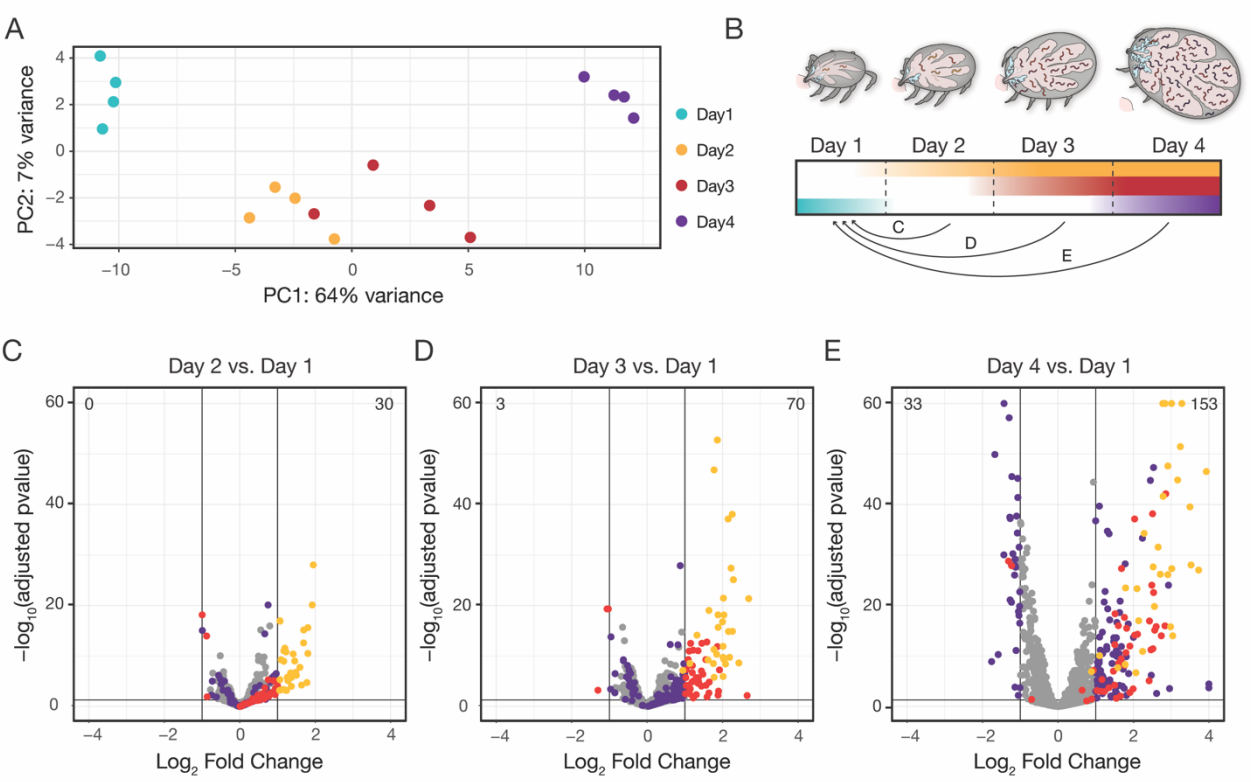

Figure 2. Global *ex vivo* profiling of *Bb* reveals extent and kinetics of transcriptional changes. (**A**) Principal component analysis of samples from across feeding. PC1 correlates strongly with day of feeding. (**B**) Schematic depicting how data was analyzed, as pairwise comparisons between the first day after attachment and all other days. (**C-E**) Volcano plots of differentially expressed genes of day 2 versus day 1 after attachment (**C**), day 3 versus day 1 (**D**), and day 4 versus day 1 (**E**). The total number of upregulated genes is shown in the top right and downregulated genes is shown in the top left. Yellow dots are genes that change expression between day 1 and day 2, red dots are genes that change expression between day 1 and day 3, and purple dots are genes that change expression between day 1 and day 4. Two genes with $\log_2$ fold changes >4 are shown at 4, and five genes with -$\log_{10}$(padj) >60 are shown at 60. Only genes with at least a 2-fold change are highlighted. p-value < 0.05, Wald tests. By day 4 of feeding, 153 genes are upregulated and 33 genes are downregulated from day 1 baseline levels.

genes changed suddenly over the course of feeding, while others were more gradual. To our knowledge, this is the first comprehensive report of global *Bb* expression changes within feeding ticks.

To help assess the integrity of our dataset, we examined expression profiles for previously characterized targets of major transcriptional programs activated at the onset of the bloodmeal, the Hk1/Rrp1 two-component system and the RpoN/RpoS sigma factor cascade (Caimano et al., 2019, 2015). Between day 1 and day 4, the majority of genes previously reported to be activated or repressed by Rrp1 *in vitro* (Caimano et al., 2015) trended significantly in the expected direction *ex vivo* (111/148 upregulated, 37/57 downregulated, p<0.05, Wald tests, **Figure S3A**). The majority of the genes previously reported to be activated by RpoS in a mammalian context, including canonical targets *ospC* and *dbpA*, were also significantly upregulated during tick feeding (33/55, p<0.05, Wald tests) (**Figure S3B**), along with *rpoS* itself (**Figure S3C**), as expected (Hübner et al., 2001). However, very few genes repressed by RpoS in mammals were similarly repressed in ticks (2/33, p<0.05, Wald tests). These data support the hypothesis that while RpoS-dependent gene activation occurs across both vertebrate and vector stages of *Bb* transmission, RpoS-dependent repression is specific to spirochetes infecting a mammalian host (Caimano et

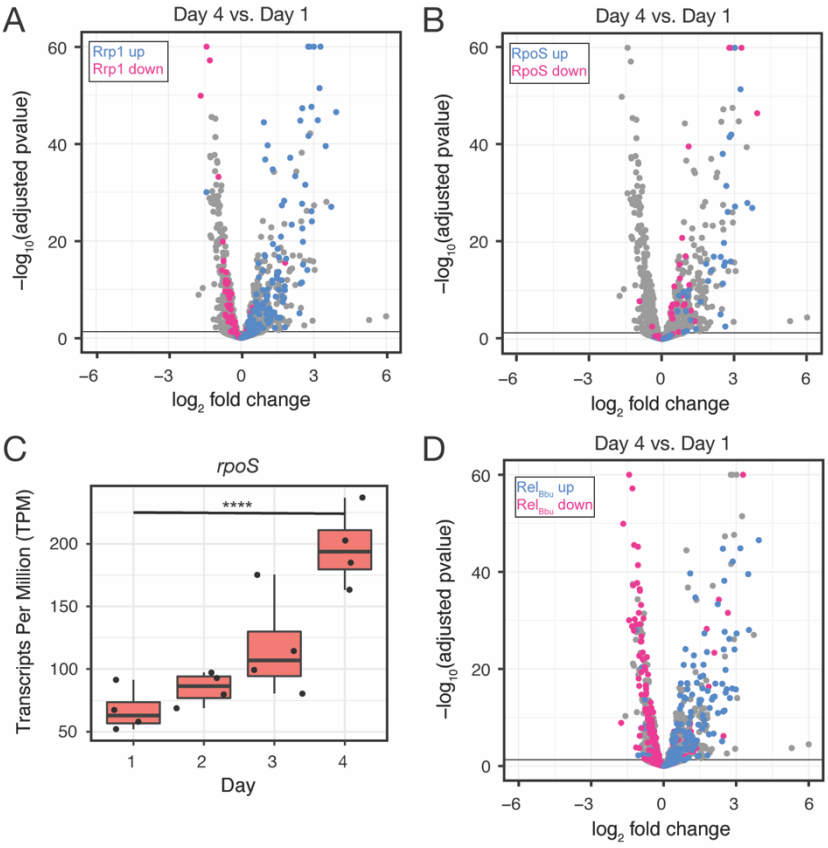

Figure S3. *Ex vivo* RNA-seq corroborates key transcriptional programs in the tick. (**A**) Volcano plot of DE genes comparing day 4 to day 1, with Rrp1-upregulated (blue) and downregulated (pink) genes. Rrp1-regulated genes correlate well with up and downregulated genes during feeding. (**B**) Volcano plot of DE genes comparing day 4 to day 1, with RpoS-upregulated (blue) and downregulated (pink) genes. Genes upregulated by RpoS in mammals increase during feeding, but genes repressed by RpoS in mammals are not repressed in the tick. (**C**) Tukey style boxplot of Transcripts Per Million (TPM) on each day for *rpoS*. Black dots represent replicates. ****p-value < 0.00001, Wald test. *rpoS* expression increases over the course of feeding. (**D**) Volcano plot of DE genes comparing day 4 to day 1, with Rel_{Bbu}-upregulated (blue) and downregulated (pink) genes. About half of Rel_{Bbu} genes change in the expected direction over feeding.

al., 2019, 2007). We also compared our DE genes to those regulated by Rel_{Bbu} as part of the stringent response, another major transcriptional program active in *Bb* in the tick during nutrient starvation (Drecktrah et al., 2015). About half of Rel_{Bbu}-regulated genes changed in the direction expected if the stringent response was active during this time (**Figure S3D**); however, more of the genes that were downregulated over feeding have been reported to be regulated by Rel_{Bbu} than either RpoS or Rrp1, suggesting it may play some role during feeding.

By looking at these previously reported transcriptional regulons in our data, we were able to verify that our data captured expected transcriptional programs active during tick feeding. Nevertheless, 25% of the twofold DE genes were not previously identified through these RNA-seq studies as dependent upon RpoS, Rrp1, or Rel_{Bbu} (Caimano et al., 2019, 2015; Drecktrah et al., 2015), which are the three main *Bb* regulatory programs active in the tick (Samuels et al., 2021). These additional genes highlight the necessity of measuring transcription in the tick environment and suggest we uncovered gene expression changes specific to the tick-stage of the *Bb* enzootic cycle. The nature and dynamics of these changes provide insights into potential genetic determinants of *Bb* survival, proliferation, and dissemination in the tick during transmission.

***Bb* genes upregulated during feeding are found predominantly on plasmids**

Bb has a complex, highly fragmented genome (Barbour, 1988) (**Figure 3A**), including numerous plasmids that are necessary during specific stages of the enzootic cycle (reviewed in Schwartz et al., 2021) suggesting they contain genes that are crucial for pathogen transmission and survival. In fact, many genes found on the plasmids have been previously shown to alter expression upon environmental changes or in different host environments (Iyer et al., 2015; Ojaimi et al., 2005; Revel et al., 2002; Tokarz et al., 2004). Thus, we reasoned that many of the 192 *Bb* genes that change expression over the course of the tick bloodmeal would reside on the plasmids, and we examined their distribution throughout the genome. Consistent with these previous reports, we found that most of the upregulated genes were located on the plasmids (143/158; 90%), while fewer were found on the chromosome (15/158; 10%) (**Figure 3B**), which is home to the majority of metabolic and other housekeeping genes. In contrast, the majority of the downregulated genes were found on the chromosome (27/34, 79%) (**Fig 3C**).

Several plasmid-encoded genes that were longitudinally upregulated in our datasets have known roles during the tick bloodmeal or in mammalian infection. For example, linear plasmid 54 (lp54),

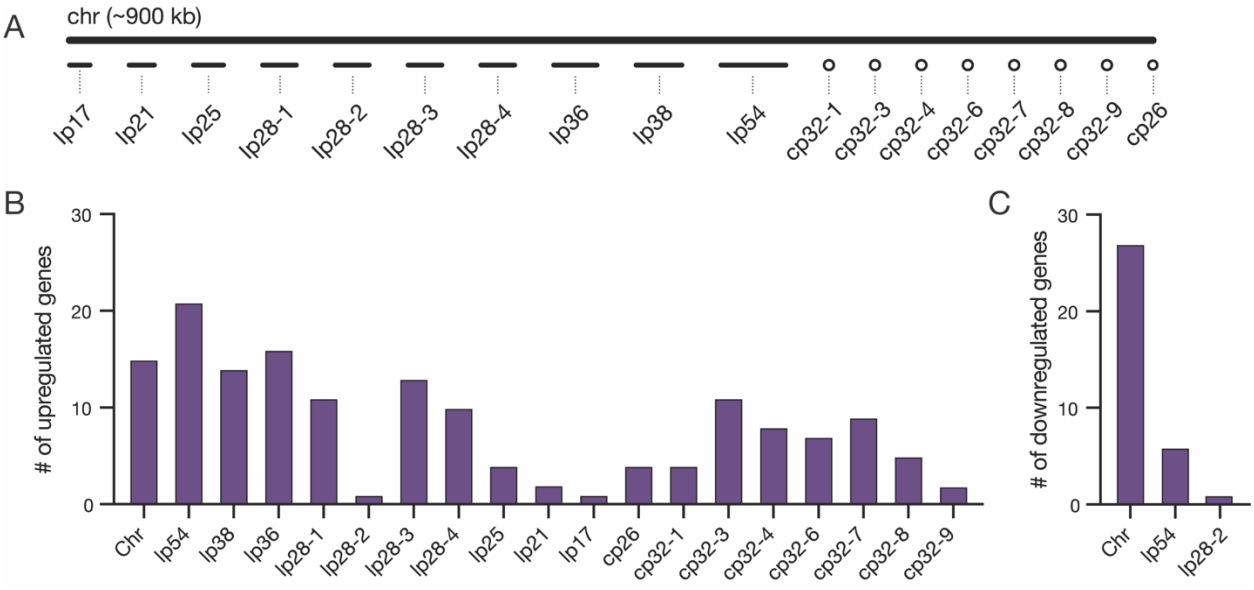

Figure 3. *Bb* genes upregulated during feeding are found predominantly on plasmids. (**A**) Schematic of the chromosome and plasmids in the *Bb* B31-S9 genome. (**B-C**) The number of genes from each chromosome or plasmid that increased (**B**) or decreased expression (**C**) twofold during feeding. Upregulated genes are distributed across plasmids, while downregulated genes are found on the chromosome and lp54.

which is an essential plasmid present in all *Bb* isolates (Casjens et al., 2012), contained the largest number of upregulated genes. Many of the genes on lp54 are known to be regulated by RpoS during feeding, including those encoding adhesins DbpA and DbpB, which are important for infectivity in the host (Blevins et al., 2008). This set also included five members of a paralogous family of outer surface lipoproteins BBA64, BBA65, BBA66, BBA71, and BBA73. BBA64 and BBA66 are necessary for optimal transmission via the tick bite (Gilmore et al., 2010; Patton et al., 2013). These findings indicate our dataset captures key *Bb* transcriptional responses known to be important for survival inside the tick during a bloodmeal.

Many upregulated genes were encoded by cp32 plasmid prophages. *Bb* strain B31-S9 harbors seven cp32 isoforms that are highly similar to each other (Casjens et al., 2012). When cp32 prophages are induced, phage virions called ϕBB1 are produced (Eggers and Samuels, 1999). In addition to phage structural genes, cp32 contain loci that encode various families of paralogous outer surface proteins (Stevenson et al., 2000). Amongst the cp32 genes that increased over feeding were members of the RevA, Erp, and Mlp families, which are known to increase expression during the bloodmeal (Gilmore et al., 2001). We also found several phage genes that were upregulated, including those encoding proteins annotated as phage terminases on cp32-3, cp32-4, and cp32-7 (BBS45, BBR45, and BBO44). Some cp32 genes have been shown to change expression in response to temperature changes (Tokarz et al., 2004) and as a part of the stringent response regulated by Rel_{Bbu} (Drecktrah et al., 2015). Our data suggest that some

prophage genes are upregulated over the course of tick feeding, raising the possibility that cp32 prophage are induced towards the end of feeding. Overall, our data support the long-held idea that the *Bb* plasmids, which house many genes encoding cell envelope proteins, proteins of unknown function, and prophage genes, play a critical role in the enzootic cycle during the key transition period of tick feeding.

***Bb* genes encoding outer surface proteins are enriched among upregulated genes**

To gain a better overall sense of the types of genes that changed over feeding and the timing of those changes, we grouped DE genes into functional categories. Since a high proportion of plasmid genes encode lipoproteins within the unique protein-rich outer surface of *Bb*, genes of unknown function, and predicted prophage genes (Casjens et al., 2000; Fraser et al., 1997), we expected that many of the DE genes would fall into these categories. We classified the genes as related to either: cell envelope, bacteriophage, cell division, DNA replication and repair, chemotaxis and motility, metabolism, transporter proteins, transcription, translation, stress response, protein degradation, or unknown (as in Drecktrah et al., 2015)(see **Table S4**).

Of the genes that increased at least twofold over feeding, the clear majority each day of feeding fell into two broad categories, cell envelope (55 of 158 total genes) and proteins of unknown function (69 of 158 total genes), with fewer genes related to metabolism, chemotaxis and motility, transporters, bacteriophage, cell division, and transcription (**Figure 4A**). In contrast to the upregulated genes, genes downregulated during feeding were more evenly distributed among the functional categories – including translation, protein degradation, transcription, and metabolism – consistent with many of them being located on the chromosome.

When looking at changes across these functional categories, the overrepresentation of cell envelope proteins was striking, while not unexpected. The *Bb* outer surface is covered with lipoproteins (**Figure 4B**), and these proteins are critical determinants in *Bb* interactions with the various environments encountered during the enzootic cycle (Kurokawa et al., 2020). We found that more than half of these outer surface lipoproteins changed expression during this time, with 46 of 83 total outer surface lipoproteins (Dowdell et al., 2017) differentially expressed twofold over feeding (**Figure 4C**). These data suggested widespread changes may be occurring on the *Bb* outer surface during feeding.

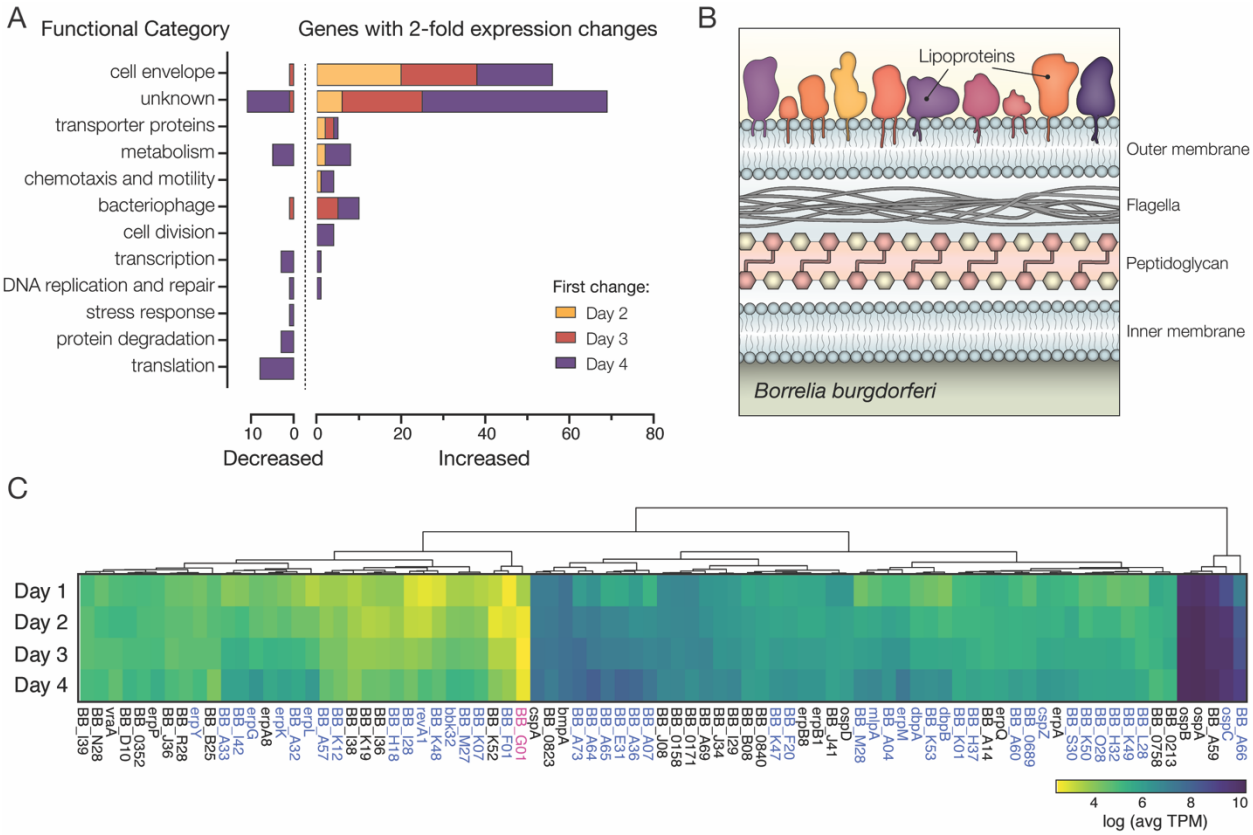

Figure 4. *Bb* genes encoding outer surface proteins are enriched among upregulated genes. (**A**) The number of *Bb* genes that change over the course of tick feeding sorted into functional categories. Genes that first change 2 days after attachment are shown in yellow, 3 days after attachment in red, and 4 days after attachment in purple. A majority of upregulated genes fall into cell envelope and unknown categories. (**B**) Schematic of the outer membrane of *Bb* showing the location of outer surface lipoproteins. (**C**) Heat map of the average Transcripts Per Million (TPM) of all genes encoding outer surface lipoproteins across the 4 days of tick feeding. Genes in blue were twofold upregulated and genes in pink twofold downregulated over feeding. A majority of genes encoding outer surface proteins increased in expression throughout feeding, while having different magnitudes of expression.

To understand the functional implications of expression changes in a majority of outer surface lipoproteins, we also compared their relative expression. The magnitude of expression varied greatly, with *ospA*, *ospB*, *ospC*, and *bba59* being the most highly expressed outer surface protein transcripts. Many of the outer surface protein genes that we found increased expression over feeding were much less abundantly expressed (**Table S5**). However, even the genes that appeared to have low expression in these population level measurements could play important roles in transmission if they are highly expressed in a small number of crucial cells, such as those that ultimately escape the midgut. While bulk RNA-seq cannot distinguish what is happening at the single cell level, our data suggest that during the bloodmeal, *Bb* are undergoing a complex outer surface transformation driven by increases in a majority of the genes encoding these crucial lipoproteins.

Identification of candidate tick interaction partners of *Bb* cells *ex vivo*

Our RNA-seq data suggested that the outer surface of *Bb* transforms over the course of feeding as *Bb* are primed for transmission to a vertebrate host. At the same time, the tick midgut environment is changing as the tick begins to digest its bloodmeal. Tick-*Bb* interactions are likely crucial at the beginning of the tick bloodmeal, as *Bb* adhere to the tick gut epithelium before becoming motile and migrating out of the midgut and into the salivary glands (Dunham-Ems et al., 2009). Some *Bb* outer surface proteins, such as BBE31 and BBA52 play key roles in pathogen migration through interactions with the tick environment (Kurokawa et al., 2020). We wanted to explore the changing tick environment to identify tick proteins with which *Bb* could interact throughout the tick bloodmeal. Since our *Bb* enrichment process retained some tick material, we reasoned that tick proteins that interact with *Bb* would be present in these samples.

To outline the changes occurring in the tick during feeding and to identify candidate *Bb*-interacting tick proteins, we used mass spectrometry to survey the content of the tick material that was enriched along with the *Bb* cells we sequenced at early and late stages during feeding. We purified proteins from the α*Bb*-enriched fraction of crushed infected ticks on day 1 after attachment and day 4 after attachment in triplicate. As controls for each day, we also performed the *Bb* enrichment process on lysate from uninfected ticks mixed with *in vitro* cultured *Bb* to help rule out proteins

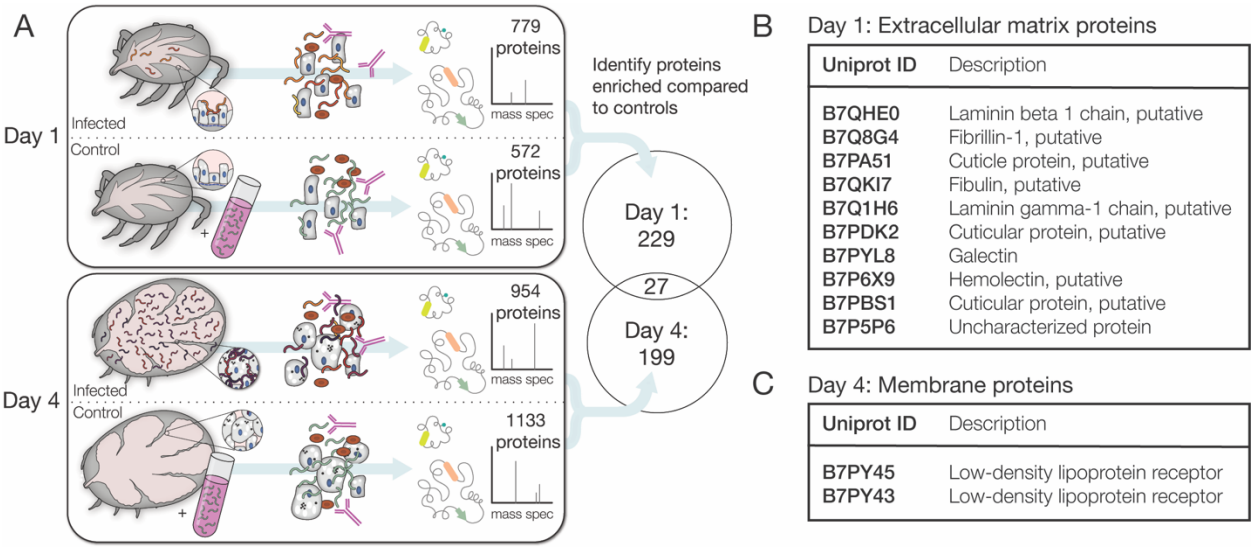

Figure 5. Identification of candidate tick interaction partners of *Bb* cells *ex vivo*. (**A**) Schematic of experiment to determine candidate tick proteins interacting with *Bb* over the course of feeding. Ticks were collected 1 day after attachment and 4 days after attachment. Uninfected ticks at the same time points were mixed with cultured *Bb* as controls. *Bb* was enriched with anti-*Bb* antibody as in RNA-seq experiments and then subjected to mass spectrometry to identify tick proteins present in the samples. Venn diagram depicts the proteins enriched in day 1 and day 4 samples over controls. Tick proteins that are enriched with *Bb* vary greatly over the course of feeding. (**B**) Tick proteins uniquely identified one day after attachment that are annotated as extracellular matrix (ECM) proteins. (**C**) Tick proteins uniquely identified four days after attachment that are annotated as low-density lipoprotein receptors. ECM and membrane proteins may be good candidates for *Bb*-interacting proteins.

that were not pulled down through *in vivo* tick-*Bb* interactions (**Figure 5A**). We identified between 414 and 2240 protein groups per sample replicate. To identify proteins of interest, we looked for those that were detected in at least two of three replicates with infected ticks and had a mean average coverage twice that of uninfected ticks mixed with cultured *Bb*. We found 256 proteins that were enriched with *Bb* from infected ticks one day after attachment and 226 proteins that were enriched with *Bb* from infected ticks four days after attachment (**Table S6**). Of these proteins, only 27 were detectable on both days, suggesting the tick proteins present upon *Bb* enrichment change dramatically over the course of feeding. The vast majority of all detected proteins were from ticks (98%). Amongst the small number of *Bb* proteins, we identified OspC in the samples from day 4 after attachment but not day 1 after attachment, confirming the expression change we saw in our RNA-seq. The distinct sets of tick proteins we identified at each timepoint suggest dramatic changes occur in the *Bb*-infected tick midgut environment during feeding that may alter the landscape of tick-*Bb* interactions.

Some of the proteins enriched with *Bb* from the tick may be good candidates for key *Bb*-interacting partners during feeding, especially if they are localized to the surface of tick cells where they may encounter *Bb*. The scarcity of both predicted and experimentally validated functions and localizations for tick proteins makes it difficult to fully assess the potential for tick protein interactions with extracellular *Bb*. Nevertheless, of the proteins found exclusively one day after attachment, 10 were categorized as extracellular matrix proteins using the PANTHER gene database (Thomas et al., 2022), and this category was statistically enriched (Fisher's exact test, FDR=0.000093) (**Figure 5B, Table S7**). 30 additional proteins were annotated with a cellular component as plasma membrane. Four days after attachment, we did not detect any annotated extracellular matrix proteins; however, we identified 31 proteins that are likely to be found at the membrane, including two proteins annotated as putative low-density lipoprotein receptors (**Figure 5C, Table S8**). These extracellular matrix and membrane proteins may be the most likely to directly interact with *Bb* during this timeframe and are candidates for tick proteins important in the *Bb* dissemination process. The proteins present in the changing tick environment may be key determinants of pathogen transmission as *Bb* remodels its outer surface while preparing to migrate through the tick to a new host.

DISCUSSION

Vector-borne pathogens must adapt to distinct environments as they are transmitted by arthropods to colonize new bloodmeal hosts. The tick-borne Lyme disease pathogen *Bb*

355 undergoes transcriptional changes inside its vector over the course of a single bloodmeal that are
356 important for a number of key transmission events. For example, expression changes enable
357 survival in the feeding tick (He et al., 2011), facilitate transmission across several internal
358 compartments into the bloodmeal host (Kurokawa et al., 2020), and prime bacteria for successful
359 infection of the next host (Kasumba et al., 2016). Capturing these changes as they occur *in vivo*
360 has been challenging due to the low relative abundance of *Bb* material inside of the rapidly
361 growing, blood-filled tick. To date, many advances in our understanding of *Bb* expression during
362 transmission have come from tracking changes in small subsets of genes during tick feeding
363 (Gilmore et al., 2001), leveraging *Bb* culture conditions that approximate environmental changes
364 across its lifecycle (Ojaimi et al., 2005; Revel et al., 2002; Tokarz et al., 2004), and defining
365 transcriptional regulons outside of the tick (Caimano et al., 2019, 2015; Drecktrah et al., 2015).
366 Here, we developed an experimental RNA-seq-based strategy to more directly and longitudinally
367 profile gene expression for *Bb* populations isolated from ticks over the course of a transmitting
368 bloodmeal.
369
370 Our longitudinal collection of transcriptomes for *Bb* cells isolated from ticks serves as a resource
371 and starting point for delineating the functional determinants of *Bb* adaptation and transmission.
372 Our transcriptome profiles reveal more extensive expression changes for *Bb* outer surface
373 proteins than previously appreciated. These results raise the possibility that *Bb* is actively
374 remodeling its outer coat to navigate the dynamic tick environment during feeding, akin to
375 wardrobe changes across seasons. These outer surface changes may play roles in the
376 persistence of *Bb* in the tick, cell adhesion, or in immune evasion, either inside of the tick or later
377 in the vertebrate host (Kenedy et al., 2012). It has long been observed that molecular interactions
378 between pathogens and the midgut of their vectors are key determinants of transmission (Barillas-
379 Mury et al., 2022). Modifications to the *Bb* surface could facilitate different tick–pathogen
380 interactions that are critical for its physical movement through tick compartments. Notably, we
381 also identified numerous genes of unknown function that change expression during feeding.
382 Although challenging to address, efforts focused on uncovering the contribution of these genes
383 to the *Bb* life cycle could be groundbreaking for understanding the unique aspects of tick-borne
384 transmission.
385
386 More comprehensive knowledge about *Bb* outer surface proteins and their functional
387 consequences could lead to new avenues for curtailing the spread of Lyme disease. Protective
388 vaccines against vector-borne pathogens have often targeted surface proteins encoded by

pathogens (Kovacs-Simon et al., 2010). While previous Lyme disease vaccine efforts effectively targeted the highly expressed *Bb* outer surface protein OspA (Steere et al., 1998), more targets could increase the likelihood of a successful vaccine. Our study provides a catalog of new *Bb* candidates that could be explored. In addition, our biochemical pull-downs using tick-isolated *Bb* cells as bait unearthed a preliminary list of potential tick proteins that could be involved in tick–*Bb* molecular interactions. Blocking molecular interactions that are functionally critical for transmission could also be explored as a therapeutic strategy (Barillas-Mury et al., 2022; Manning and Cantaert, 2019).

Our transcriptomic resource provides critical insights into *Bb* population-level changes during the vector stage of its lifecycle, an important starting point for understanding the primary drivers of tick-borne transmission. Strikingly few *Bb* cells out of the total pathogen population in ticks are ultimately transmitted to the next host during feeding. There are several major bottlenecks to infection, including dissemination to the tick salivary glands and survival upon inoculation of the host (Dunham-Ems et al., 2009; Rego et al., 2014). There may be important physiological or molecular variations across *Bb* cells within the population residing in the tick that contribute to these differential outcomes. An important clue is the fact that *Bb* proteins are indeed heterogeneously expressed across cells within the feeding tick midgut (Ohnishi et al., 2001). Conducting transcriptomic analyses at the single-cell level will be key. Given that only a small number of *Bb* escape the tick midgut, genes that appear unaltered or show low expression levels across the bulk population could still play an outsized role in infection for a minority of the cells. Our work provides a foundational methodology that can be leveraged to greatly improve the resolution of tick–microbe studies. Technological advances stemming from this work will provide molecular details that potentiate new questions and may unearth surprising mechanistic insights into the unique lifestyles of tick-borne pathogens.

METHODS

B. burgdorferi culture

Bb strain B31-S9 (Rego et al., 2011) was provided by Dr. Patricia Rosa (NIAID, NIH, RML) and cultured in BSK II media at 35°C, 2.5% CO_2.

Tick feeding experiments

I. scapularis larvae were purchased from the Tick Lab at Oklahoma State University (OSU) (for RNA-seq experiments) or provided by BEI Resources, a division of the Center for Disease Control

(for mass spectrometry experiments). Before and after feeding, ticks were maintained in glass jars with a relative humidity of 95% (saturated solution of potassium nitrate) in a sealed incubator at 22°C with a light cycle of 16h/8h (light/dark). Animal experiments were conducted in accordance with the approval of the Institutional Animal Care and Use Committee (IACUC) at UCSF. Ticks were fed on young (4–6-week-old) female C3H/HeJ mice acquired from Jackson Laboratories. Mice were anesthetized with ketamine/xylazine before placement of ≤ 100 larval or ≤ 30 nymphal ticks. Ticks were either pulled off isoflurane anesthetized mice at various times during feeding (1-3 days after placement) or allowed to feed to repletion and collected from mouse cages. Replete larval ticks were placed in the incubator to molt before being used as nymphs in experiments.

Western blot with anti-*Bb* antibody

To determine whether the anti-*Bb* antibody targeted ospA, we cultured wildtype *Bb* (B31-A3), ospA1-mutants (ospA1) and ospA-restored *Bb* (ospA^{+}B1) (Battisti et al., 2008) to approximately 5x10^{7} *Bb*/mL and centrifuged 3 mLs of culture for 7 minutes at 8000 x g, washing twice with PBS. Pelleted cells were lysed in 50 µL of water, and 25 ng per sample was mixed with 5X loading dye (0.25% Bromophenol Blue, 50% Glycerol, 10% Sodium Dodecyl Sulfate, 0.25M Tris-Cl pH 6.8, 10% B-Mercaptoethanol), run on a Mini-PROTEAN TGX 4-15% gel (Biorad), and transferred using the Trans-Blot Turbo Transfer System (Biorad). After transfer, the blot was blocked for 30 minutes at 4°C in TBST (Tris buffered saline with .1% tween) with 5% milk, then treated with anti-*Bb* antibody (Invitrogen: PA1-73004; RRID: AB_1016668) diluted 1:10,000 for 1 hour at room temperature, followed by anti-rabbit HRP secondary antibody (Advansta) diluted 1:5,000 for 45 minutes at room temperature with short PBST washes between each step. Blots were exposed using Clarity Western ECL Substrate (Biorad) and imaged using the Azure C400 imaging system (Azure Biosystems). This experiment was repeated three times.

Enrichment of *Bb* from feeding ticks

To sequence RNA from *Bb* from feeding ticks, we enriched *Bb* to increase the ratio of *Bb* to tick material. Larval ticks were fed to repletion on three mice that were infected with *Bb* through intraperitoneal and subcutaneous injection with 10^{4} total *Bb*. Approximately five months later, the molted nymphal ticks were fed on eight mice. We estimated that 83% of the ticks were infected with *Bb* by crushing 12 unfed nymphs in BSK II media and checking for viable *Bb* days later. Ticks were pulled from all mice and pooled into four replicates 1 day after placement (14 ticks per replicate), 2 days after placement (12 ticks per replicate), and 3 days after placement (6 ticks per

457 replicate) and collected from cages 4 days after placement (7 ticks per replicate). Shortly after
458 collection, ticks were washed with water and placed in a 2 mL glass dounce grinder (Kimble) in
459 500 µL of phosphate-buffered saline (PBS). Ticks were homogenized first with the large clearance
460 pestle and then the small clearance pestle. The homogenate was transferred to a 1.5 mL
461 Eppendorf tube and 500 µL of PBS was added to total 1 mL. At this stage, 50 µL of homogenate
462 was removed as an input sample and mixed with 500 µL of TRIzol (Invitrogen) for RNA extraction.
463 2 µL of anti-*Bb* antibody (Invitrogen: PA1-73004; RRID: AB_1016668) was added to the
464 homogenate, which was then placed on a nutator at 4°C for 30 minutes. During incubation, 50 µL
465 of Dynabeads Protein G (Invitrogen) per sample were washed twice in PBS. After incubation with
466 the antibody, the homogenate and antibody mixture were added to the beads. This mixture was
467 placed on a nutator at 4°C for 30 minutes. Tubes were then placed on a magnet to secure beads,
468 and the homogenate was removed and saved to create depleted samples. The depleted
469 homogenate was centrifuged at 8,000 x g for 7 minutes, 900 µL of supernatant was removed, and
470 500 µL of TRIzol was added to the pellet to create depleted samples. The beads were washed
471 twice with 1 mL of PBS, resuspending the beads each time. The second wash was removed and
472 500 µL of TRIzol was added to the beads to create enriched samples. RNA was extracted from
473 all input, enriched, and depleted samples using the Zymo Direct-zol RNA Microprep Kit with on-
474 column DNase treatment (Zymo Research). The step-by-step *Bb* enrichment protocol is available
475 at: https://www.protocols.io/view/b-burgdorferi-enrichment-from-feeding-ticks-36wgqjrbovk5/v1
476
477 **Enrichment of *Bb* from culture**
478 To test whether the *Bb* enrichment process altered gene expression levels, we performed the
479 enrichment protocol on cultured *Bb*. We grew three tubes of *Bb* in BSK II media to $9x10^4$ *Bb*/mL
480 at 35°C. 1 mL of culture was spun down at 8,000 x g for 7 minutes, media was removed, *Bb* were
481 washed in 1 mL of PBS and spun again. Pelleted *Bb* were resuspended in 1 mL of fresh PBS.
482 These samples were used as starting homogenate for the *Bb* enrichment protocol and input,
483 enriched, and depleted fractions were collected as above. RNA-seq libraries from these samples
484 were prepared and sequenced as below.
485
486 **RNA-seq library preparation and sequencing**
487 To make RNA-seq libraries from enriched *Bb* RNA, we used 50 ng of total RNA as input into the
488 NEBNext Ultra II Directional RNA Library Prep Kit for Illumina (New England BioLabs). We
489 prepared libraries following the manufacturer's protocol for use of the kit with purified mRNA or

rRNA-depleted RNA, despite starting with total RNA. Libraries were barcoded using NEBNext Multiplex Oligos for Illumina Dual Index (New England BioLabs).

To deplete reads from the libraries that were from tick, *Bb*, or mouse rRNA, we used Depletion of Abundant Sequences by Hybridization (DASH) (Gu et al., 2016), which targets Cas9 to unwanted reads in RNA-seq libraries using custom dual-guide RNAs (dgRNAs). Our dgRNAs targeted short sequences within tick rRNA, mouse rRNA, and *Bb* rRNA that were designed using DASHit software (Dynerman et al., 2020). We ordered crRNAs that targeted our sequences of interest (Ring et al., 2022). To transcribe the dgRNAs, we followed our protocol for In Vitro Transcription for dgRNA V2 (Lyden et al., 2019b). Both tracrRNA and pooled crRNA DNA templates were annealed to equimolar amounts of T7 primer by heating to 95°C for 2 minutes and slowly cooling to room temperature. Annealed templates were used in 1 mL in vitro transcription reactions with: 120 µL10X T7 buffer (400 mM Tris pH 7.9, 200 mM MgCl2, 50 mM DTT, 20 mM spermidine (Sigma)), 100 µL of T7 enzyme (custom prepped enzyme from E. Crawford, diluted 1:100 in T7 buffer, final concentration: 100 µg/mL), 300 µl NTPs (25 mM each, Thermo Fisher Scientific), 4 µg of annealed crRNA template or 8 µg of annealed tracrRNA template, and water to 1 mL. In vitro transcription was performed for 2 hours at 37°C. Reactions were purified twice with the Zymo RNA Clean & Concentrator-5 Kit (Zymo Research). To form the dgRNA complex for DASH, crRNA and tracrRNAs were diluted to 80 µM, mixed in equimolar amounts and annealed by heating to 95ºC for 30 seconds and cooling slowly to room temperature.

After transcription of dgRNAs, we performed DASH Protocol Version 4 (Lyden et al., 2019a) on each library individually. Cas9 and transcribed dgRNAs were prepped by mixing: 2.5 µL 10X Cas9 buffer, 5 µL Cas9 (New England BioLabs), and 5 µL of 40 µM transcribed dgRNAs. The mixture was incubated at 37°C for 5 minutes before 7.5 µL of RNA-seq library (2.8 nM) was added. The mixture was incubated at 37°C for 1 hour and then purified with Zymo DNA Clean & Concentrator-5 (Zymo Research) following the PCR product protocol and eluting DNA into 10.5 µL of water. During cleanup, Cas9 was again mixed with buffer and dgRNAs and incubated at 37°C for 5 minutes. Following cleanup, eluted DNA was added to the second Cas9-dgRNA mixture and incubated at 37°C for 1 hour for a second time. Then, 1 µL of proteinase K (New England Biolabs) was added, and the mixture was incubated at 50°C for 15 min. The libraries were then purified with 0.9x volume of sparQ PureMag Beads (QuantaBio) following the standard protocol, eluting in 24 µL of water. rRNA-depleted RNA-seq libraries were then amplified in a BioRad CFX96 using the Kapa HiFi Real-Time Amplification Kit in a 50 µL reaction with 25 µL master mix, 23 µL of the

DASHed library pool, and 2 µL of 25 µM mix of Illumina P5 (5'-AATGATACGGCGACCACCGAGATCT) and P7 (5'- CAAGCAGAAGACGGCATACGAGAT) primers. The qPCR program for amplification was as follows: 98°C for 45 sec (1 cycle), (98°C for 15 sec, 63°C for 30 sec, 72°C for 45 sec, plate read, 72°C for 20 sec) for 10 cycles (day 3 and day 4 samples) or 11 cycles (day 1 and day 2 samples). The libraries were removed from cycling conditions before leaving the exponential phase of amplification and then purified with 0.9X volume of sparQ PureMag Beads according to the standard protocol.

Following DASH, RNA-seq libraries were sequenced on an Illumina NovaSeq S2 (2 lanes) with paired-end 100 base pair reads. Libraries from *in vitro* cultured control experiment were sequenced on an Illumina NextSeq with paired-end 75 base pair reads. FASTQ files and raw *Bb* read counts for *in vitro* control experiment (GSE217146) and *ex vivo* experiment (GSE216261) have been deposited in NCBI's Gene Expression Omnibus (Edgar et al., 2002) under SuperSeries accession number GSE217236.

RNA-seq data analysis

To measure the success of our rRNA depletion through DASH, we used DASHit software (Dynerman et al., 2020) to determine the percentage of reads that would be DASHable by our guide RNAs (Ring et al., 2022). For pre-DASH data, we sequenced the input of each of our RNA-seq libraries before performing DASH on a MiSeq V2 Micro (Illumina). We tested DASHability on a random subset of 200,000 paired-end reads chosen by seqtk (https://github.com/lh3/seqtk) from each pre- and post-DASH library.

To map our RNA-seq data to *Bb*, we wanted to optimize for mapping reads that came from the many paralogous gene families found across the plasmids of the genome. We used the pseudoalignment tool Salmon v1.2.1 (Patro et al., 2017), which is used to accurately map reads coming from different isoforms of the same gene, for this reason. While using Salmon to map to CDS sequences may improve mapping to paralogous genes, it may also have a tradeoff of reduced mapping of reads that fall on the ends of genes that reside in operons. Nevertheless, all samples should be similarly affected, and any undercounting should not change differential expression results. Reads were first trimmed of bases with quality scores less than 20 using Trim Galore v0.6.5 (https://github.com/FelixKrueger/TrimGalore). We mapped our reads to *Bb* CDS sequences as a reference transcriptome: NCBI Genbank GCA_000008685.2 ASM868v2 (with plasmids lp5, cp9, and lp56 removed as they are not present in B31-S9) using Salmon with the following parameters: --validateMappings --seqBias --gcBias. Before mapping, the transcriptome

was first indexed using the Salmon index command with the whole genome as decoys and the parameter --keepDuplicates to keep all duplicate genes.

Read counts from Salmon were used as input into DESeq2 v1.24.0 (Love et al., 2014) for differential expression analysis in R version 3.6.1. DESeq2 function PlotPCA() was used to create a PCA plot from read counts after running the varianceStabilizingTransformation() function. For differential expression analysis between days, a DESeq object was created from count data using the DESeq() function. The lfcShrink() function with the apeglm method (Zhu et al., 2018) was used to calculate fold changes between days. Code used for differential expression analysis is available at https://github.com/annesapiro/Bb-tick-feeding.

Gene classification

To classify genes into functional groups, functional categories were sourced from Drecktrah et al., 2015 where available. Other gene functions were sourced from Fraser et al., 1997. Genes found within the co-transcribed “late” bacteriophage operon (Zhang and Marconi, 2005) were considered “bacteriophage” even if their function is unknown. Outer surface lipoproteins were those found in Dowdell et al., 2017 plus additional lipoproteins listed in Iyer et al., 2015 that were found in Dowdell et al. 2017 categories SpII and SpI and evidence of outer surface localization. Outer surface and periplasmic lipoproteins were classified as “cell envelope” in the absence of other classifications. Gene family information from Casjens et al., 2000 was considered to aid in classification.

RT-qPCR measuring *Bb* enrichment

To test the efficacy of our enrichment protocol, we used RT-qPCR to quantify *Bb flaB* and *I. scapularis gapdh* transcript levels in enriched and depleted fractions. We synthesized cDNA from 8 µL of RNA extracted from *Bb* enrichment samples and their matched depleted samples from feeding day 2, day 3, and day 4 using the qScript cDNA Synthesis Kit (Quantabio). cDNA was diluted 2X before use in qPCR. To measure *flaB* copies, we created standards of known concentration from purified PCR products. These standards were made from PCR with primers with the following sequences: 5’-CACATATTCAGATGCAGACAGAGGTTCTA and 5’-GAAGGTGCTGTAGCAGGTGCTGGCTGT. We ran a dilution series with ten-fold dilutions between 10^6 copies and 10^1 copies of this PCR template alongside our enriched and depleted samples. We performed qPCR using Taqman Universal PCR Master Mix (Applied Biosystems). The primers used to amplify *flaB* were: 5’- TCTTTTCTCTGGTGAGGGAGCT and 5’-

590 TCCTTCCTGTTGAACACCCTCT (used at 900 nM) and the probe was /56-
591 FAM/AAACTGCTCAGGCTGCACCGGTTC/36-TAMSp (used at 250 nM). For tick *gapdh* RT-
592 qPCR, the cDNA samples were diluted an additional 2X. Standards of known concentration were
593 created using the qPCR primer sequences. Primer sequences were: 5'-
594 TTCATTGGAGACACCCACAG and 5'-CGTTGTCGTACCACGAGATAA (used at 900 nM). qPCR
595 was performed using PowerUp SYBR Green Master Mix (Applied Biosystems). For both *flaB* and
596 *gapdh*, the number of copies in each sample was calculated based on the standards of known
597 concentration. Three technical replicates were averaged from each of four biological replicates at
598 each time point tested. We totaled the number of copies in each matched enriched and depleted
599 fraction to calculate the fraction of *flaB* or *gapdh* that was found in either sample. All qPCR was
600 performed on the QuantStudio3 Real-Time PCR System (Applied Biosystems).
601
602 **Immunofluorescence microscopy**
603 To test whether the anti-*Bb* antibody recognized *Bb* inside of the tick, ticks at each day of feeding
604 were crushed in 50 µL of PBS. 10 µL of lysate was spotted onto slides and allowed to air dry
605 before slides were heated briefly three times over a flame. Heat fixed slides were then treated
606 with acetone for one hour. Slides were incubated with anti-*Bb* primary antibody (1:100 diluted in
607 PBS + 0.75% BSA) for 30 minutes at 37°C in a humid chamber. A control without primary antibody
608 was also used for each day. Slides were washed once in PBS for 15 minutes at room temperature,
609 then rinsed in distilled water and air dried. Anti-rabbit IgG Alexa 488 (Invitrogen) diluted 1:100 in
610 PBS + 0.75% BSA was added for 30 minutes at 37°C in a humid chamber. Slides were washed
611 in PBS for 15 minutes at room temperature three times, adding 1:100 Propidium Iodide
612 (Invitrogen) during the second wash. Slides were then rinsed with distilled water and air dried
613 before the addition of mounting media (Fluoromount-G, SouthernBiotech) and cover slips.
614 Fluorescence imaging was performed on a Nikon Ti2 inverted microscope for widefield
615 epifluorescence using a 100x/1.40 objective. Images were captured with NIS-Elements AR View
616 5.20 and then processed with ImageJ software (Schneider et al., 2012). No strong florescence
617 signal was observed on the control slides without primary antibody.
618
619 **Mass spectrometry of *Bb*-enriched samples**
620 To identify which tick proteins were found in samples after *Bb* enrichment across feeding, we fed
621 both uninfected and infected ticks on mice. We collected three replicates of uninfected ticks one
622 day after attachment (11 ticks per replicate), infected ticks one day after attachment (27 ticks per
623 replicate), uninfected ticks four days after attachment (8 ticks per replicate), and infected ticks

four days after attachment (16 ticks per replicate). Before anti-*Bb* enrichment, the uninfected tick samples were mixed with *Bb* grown in culture that was washed with PBS (3 x10^4 *Bb* one day after attachment and 3x10^6 *Bb* four days after attachment) and mixed lysates were rotated at room temperature for 30 minutes. Infected tick samples underwent the *Bb* enrichment process immediately. The enrichment process followed the same protocol used for RNA-seq. Sample volumes were increased to 1 mL as needed, and then 2 µL of anti-*Bb* antibody (Invitrogen: PA1-73004; RRID: AB_1016668) was added, and samples were rotated at 4℃ for 30 minutes. 50 µL of Dynabeads Protein G per sample were washed in PBS during this incubation and added to the lysates, which were rotated at 4°C for 30 minutes. The beads were washed twice with 1 mL of PBS, and then placed into 50 µL of lysis buffer (iST LYSE, PreOmics). Samples were boiled at 95°C for 5 minutes, and lysates were removed from beads and frozen for mass spectrometry preparation.

For mass spectrometry, a nanoElute was attached in line to a timsTOF Pro equipped with a CaptiveSpray Source (Bruker). Chromatography was conducted at 40°C through a 25 cm reversed-phase C18 column (PepSep) at a constant flowrate of 0.5 µL min−1. Mobile phase A was 98/2/0.1% water/MeCN/formic acid (v/v/v) and phase B was MeCN with 0.1% formic acid (v/v). During a 108 min method, peptides were separated by a 3-step linear gradient (5% to 30% B over 90 min, 30% to 35% B over 10 min, 35% to 95% B over 4 min) followed by a 4 min isocratic flush at 95% for 4 min before washing and a return to low organic conditions. Experiments were run as data-dependent acquisitions with ion mobility activated in PASEF mode. MS and MS/MS spectra were collected with m/z 100 to 1700 and ions with z = +1 were excluded.

Raw data files were searched using PEAKS Online Xpro 1.6 (Bioinformatics Solutions Inc.). The precursor mass error tolerance and fragment mass error tolerance were set to 20 ppm and 0.03 respectively. The trypsin digest mode was set to semi-specific and missed cleavages was set to 2. The *I. scapularis* reference proteome (Proteome ID UP000001555, taxon 6945) and *Bb* reference proteome (Proteome ID UP000001807, strain ATCC 35210/B31) was downloaded from Uniprot, totaling 21,774 entries. The *I. scapularis* proteome was the primary search reference and the *Bb* was used as a secondary to identify any bacterial proteins present. Carbamidomethylation was selected as a fixed modification. Oxidation (M) and Deamidation (NQ) was selected as a variable modification.

Experiments were performed in biological triplicate, with samples being a single run on the instrument. Proteins present in a database search (−10 log(p-value) ≥ 20, 1% peptide and protein FDR) were subjected to the following filtration process. We first filtered to include proteins found in 2 out of 3 biological replicates, within each respective day (one or four days after attachment). We calculated the mean area of proteins found in uninfected and infected samples. Proteins with missing values (i.e. not identified in a sample) were set to 1. We calculated the ratio of mean area for each protein as infected/uninfected, and enriched proteins were identified by having a infected:uninfected ratio greater than 2 within their respective feeding day (one or four days after attachment).

To classify the proteins we identified into functional groups, we used a PANTHER Overrepresentation Test (released 07/12/2022) (Mi et al., 2019) with PANTHER version 17.0 (released 02/22/2022) (Thomas et al., 2022). We used all *Ixodes scapularis* genes in the database as our reference list and analyzed the lists of proteins enriched on each day for their PANTHER Protein Class. The test type used was Fisher's Exact, calculating a false discovery rate as the correction.

Raw data files and searched datasets are available on the Mass Spectrometry Interactive Virtual Environment (MassIVE), a full member of the Proteome Xchange consortium under the identifier: MSV000090560.

SUPPLEMENTAL TABLES

Table S1. Overview of mapping statistics from 16 *Bb* sequencing samples.

Table S2. Differential expression analysis results between *in vitro* cultured *Bb* before and after *Bb* enrichment.

Table S3. Transcriptome-wide differential expression analysis results from *Bb* across tick feeding timepoints.

Table S4. Twofold differentially expressed *Bb* genes from across tick feeding timepoints.

Table S5. Transcripts per million (TPM) for all *Bb* genes across feeding timepoints.

Table S6. Mass spectrometry analysis for *Bb*-enriched samples.

Table S7. Annotation and GO term enrichment for tick proteins enriched on feeding day 1.

Table S8. Annotation and GO term enrichment for tick proteins enriched on feeding day 4.

ACKNOWLEDGMENTS

We are grateful to all members of the Chou lab for their feedback throughout the project and specifically to Fauna Yarza and Patrick Rockefeller Grimes for assistance with tick feeding and Ethel Enoex-Godonoo for administrative assistance. We thank Amy Lyden and Emily Crawford for assistance with and reagents for DASH along with Olga Botvinnik and The Chan Zuckerberg Biohub sequencing team for their input and sequencing assistance. We thank Patricia Rosa, Jenny Wachter, Scott Samuels, and Meghan Lybecker for their feedback on the project. We also thank William Hatleberg for assistance with figure schematics. This work was funded by: a Life Sciences Research Foundation fellowship from the SVCF-Wave Fund to Anne Sapiro, a Beckman Young Investigator award from the Arnold and Mabel Beckman Foundation to Balyn Zaro, grants from CZ Biohub, the Pew Biomedical Research Foundation, and NIH funding 1R01AI132851 to Seemay Chou, and NIH INBRE funding P20GM103474 to Patrick Secor and Margie Kinnersley.

COMPETING INTERESTS

Seemay Chou is president and CEO of Arcadia Biosciences.

REFERENCES

Barbour AG. 1988. Plasmid analysis of Borrelia burgdorferi, the Lyme disease agent. *J Clin Microbiol* 26:475–478. doi:10.1128/jcm.26.3.475-478.1988

Barillas-Mury C, Ribeiro JMC, Valenzuela JG. 2022. Understanding pathogen survival and transmission by arthropod vectors to prevent human disease. *Science* 377:eabc2757. doi:10.1126/science.abc2757

Battisti JM, Bono JL, Rosa PA, Schrumpf ME, Schwan TG, Policastro PF. 2008. Outer Surface Protein A Protects Lyme Disease Spirochetes from Acquired Host Immunity in the Tick Vector. *Infect Immun* 76:5228–5237. doi:10.1128/iai.00410-08

Blevins JS, Hagman KE, Norgard MV. 2008. Assessment of decorin-binding protein A to the infectivity of Borrelia burgdorferi in the murine models of needle and tick infection. *Bmc Microbiol* 8:82. doi:10.1186/1471-2180-8-82

Caimano MJ, Dunham-Ems S, Allard AM, Cassera MB, Kenedy M, Radolf JD. 2015. Cyclic di-GMP Modulates Gene Expression in Lyme Disease Spirochetes at the Tick-Mammal Interface To Promote Spirochete Survival during the Blood Meal and Tick-to-Mammal Transmission. *Infect Immun* 83:3043–3060. doi:10.1128/iai.00315-15

Caimano MJ, Groshong AM, Belperron A, Mao J, Hawley KL, Luthra A, Graham DE, Earnhart CG, Marconi RT, Bockenstedt LK, Blevins JS, Radolf JD. 2019. The RpoS Gatekeeper in Borrelia burgdorferi: An Invariant Regulatory Scheme That Promotes Spirochete Persistence in Reservoir Hosts and Niche Diversity. *Front Microbiol* 10:1923. doi:10.3389/fmicb.2019.01923

727 Caimano MJ, Iyer R, Eggers CH, Gonzalez C, Morton EA, Gilbert MA, Schwartz I, Radolf JD.
728 2007. Analysis of the RpoS regulon in Borrelia burgdorferi in response to mammalian host
729 signals provides insight into RpoS function during the enzootic cycle. *Mol Microbiol* 65:1193–
730 1217. doi:10.1111/j.1365-2958.2007.05860.x

731 Casjens S, Palmer N, Vugt RV, Huang WM, Stevenson B, Rosa P, Lathigra R, Sutton G,
732 Peterson J, Dodson RJ, Haft D, Hickey E, Gwinn M, White O, Fraser CM. 2000. A bacterial
733 genome in flux: the twelve linear and nine circular extrachromosomal DNAs in an infectious
734 isolate of the Lyme disease spirochete Borrelia burgdorferi. *Mol Microbiol* 35:490–516.
735 doi:10.1046/j.1365-2958.2000.01698.x

736 Casjens SR, Mongodin EF, Qiu W-G, Luft BJ, Schutzer SE, Gilcrease EB, Huang WM,
737 Vujadinovic M, Aron JK, Vargas LC, Freeman S, Radune D, Weidman JF, Dimitrov GI,
738 Khouri HM, Sosa JE, Halpin RA, Dunn JJ, Fraser CM. 2012. Genome Stability of Lyme
739 Disease Spirochetes: Comparative Genomics of Borrelia burgdorferi Plasmids. *Plos One*
740 7:e33280. doi:10.1371/journal.pone.0033280

741 Dowdell AS, Murphy MD, Azodi C, Swanson SK, Florens L, Chen S, Zückert WR. 2017.
742 Comprehensive Spatial Analysis of the Borrelia burgdorferi Lipoproteome Reveals a
743 Compartmentalization Bias toward the Bacterial Surface. *J Bacteriol* 199:e00658-16.
744 doi:10.1128/jb.00658-16

745 Drecktrah D, Lybecker M, Popitsch N, Rescheneder P, Hall LS, Samuels DS. 2015. The
746 Borrelia burgdorferi RelA/SpoT Homolog and Stringent Response Regulate Survival in the
747 Tick Vector and Global Gene Expression during Starvation. *Plos Pathog* 11:e1005160.
748 doi:10.1371/journal.ppat.1005160

749 Dunham-Ems SM, Caimano MJ, Pal U, Wolgemuth CW, Eggers CH, Balic A, Radolf JD. 2009.
750 Live imaging reveals a biphasic mode of dissemination of Borrelia burgdorferi within ticks. *J*
751 *Clin Invest* 119:3652–3665. doi:10.1172/jci39401

752 Dynerman D, Lyden A, Quan J, Caldera S, McGeever A, Dimitrov B, King R, Cirolia G, Tan M,
753 Sit R, Berge M van den, Kerstjens HAM, Faiz A, Christenson S, Langelier C, DeRisi J,
754 Crawford E. 2020. Designing and implementing programmable depletion in sequencing
755 libraries with DASHit. *Biorxiv* 2020.01.12.891176. doi:10.1101/2020.01.12.891176

756 Edgar R, Domrachev M, Lash AE. 2002. Gene Expression Omnibus: NCBI gene expression
757 and hybridization array data repository. *Nucleic Acids Res* 30:207–210.
758 doi:10.1093/nar/30.1.207

759 Eggers CH, Samuels DS. 1999. Molecular evidence for a new bacteriophage of Borrelia
760 burgdorferi. *J Bacteriol* 181:7308–13.

761 Fraser CM, Casjens S, Huang WM, Sutton GG, Clayton R, Lathigra R, White O, Ketchum KA,
762 Dodson R, Hickey EK, Gwinn M, Dougherty B, Tomb J-F, Fleischmann RD, Richardson D,
763 Peterson J, Kerlavage AR, Quackenbush J, Salzberg S, Hanson M, Vugt R van, Palmer N,
764 Adams MD, Gocayne J, Weidman J, Utterback T, Watthey L, McDonald L, Artiach P,
765 Bowman C, Garland S, Fujii C, Cotton MD, Horst K, Roberts K, Hatch B, Smith HO, Venter
766 JC. 1997. Genomic sequence of a Lyme disease spirochaete, Borrelia burgdorferi. *Nature*
767 390:580–586. doi:10.1038/37551

768 Gilmore RD, Howison RR, Dietrich G, Patton TG, Clifton DR, Carroll JA. 2010. The bba64 gene
769 of Borrelia burgdorferi, the Lyme disease agent, is critical for mammalian infection via tick
770 bite transmission. *P Natl Acad Sci Usa* 107:7515–20. doi:10.1073/pnas.1000268107

771 Gilmore RD, Mbow ML, Stevenson B. 2001. Analysis of Borrelia burgdorferi gene expression
772 during life cycle phases of the tick vector Ixodes scapularis. *Microbes Infect* 3:799–808.
773 doi:10.1016/s1286-4579(01)01435-6

774 Gu W, Crawford ED, O'Donovan BD, Wilson MR, Chow ED, Retallack H, DeRisi JL. 2016.
775 Depletion of Abundant Sequences by Hybridization (DASH): using Cas9 to remove
776 unwanted high-abundance species in sequencing libraries and molecular counting
777 applications. *Genome Biol* 17:41. doi:10.1186/s13059-016-0904-5

778 Haas BJ, Chin M, Nusbaum C, Birren BW, Livny J. 2012. How deep is deep enough for RNA-
779 Seq profiling of bacterial transcriptomes? *Bmc Genomics* 13:734. doi:10.1186/1471-2164-13-
780 734

781 He M, Ouyang Z, Troxell B, Xu H, Moh A, Piesman J, Norgard MV, Gomelsky M, Yang XF.
782 2011. Cyclic di-GMP is Essential for the Survival of the Lyme Disease Spirochete in Ticks.
783 *Plos Pathog* 7:e1002133. doi:10.1371/journal.ppat.1002133

784 Hübner A, Yang X, Nolen DM, Popova TG, Cabello FC, Norgard MV. 2001. Expression of
785 Borrelia burgdorferi OspC and DbpA is controlled by a RpoN–RpoS regulatory pathway. *Proc*
786 *National Acad Sci* 98:12724–12729. doi:10.1073/pnas.231442498

787 Iyer R, Caimano MJ, Luthra A, Axline D, Corona A, Iacobas DA, Radolf JD, Schwartz I. 2015.
788 Stage-specific global alterations in the transcriptomes of Lyme disease spirochetes during
789 tick feeding and following mammalian host adaptation. *Mol Microbiol* 95:509–538.
790 doi:10.1111/mmi.12882

791 Kasumba IN, Bestor A, Tilly K, Rosa PA. 2016. Virulence of the Lyme disease spirochete before
792 and after the tick bloodmeal: a quantitative assessment. *Parasite Vector* 9:129.
793 doi:10.1186/s13071-016-1380-1

794 Kenedy MR, Lenhart TR, Akins DR. 2012. The role of Borrelia burgdorferi outer surface
795 proteins. *Fems Immunol Medical Microbiol* 66:1–19. doi:10.1111/j.1574-695x.2012.00980.x

796 Kovacs-Simon A, Titball RW, Michell SL. 2010. Lipoproteins of Bacterial Pathogens. *Infect*
797 *Immun* 79:548–561. doi:10.1128/iai.00682-10

798 Kurokawa C, Lynn GE, Pedra JHF, Pal U, Narasimhan S, Fikrig E. 2020. Interactions between
799 Borrelia burgdorferi and ticks. *Nat Rev Microbiol* 1–14. doi:10.1038/s41579-020-0400-5

800 Love MI, Huber W, Anders S. 2014. Moderated estimation of fold change and dispersion for
801 RNA-seq data with DESeq2. *Genome Biol* 15:550. doi:10.1186/s13059-014-0550-8

802 Lyden A, Crawford E, Quan J, Caldera S, Dynerman D. 2019a. DASH Protocol v4.
803 doi:10.17504/protocols.io.6rjhd4n

804 Lyden A, Crawford E, Quan J, Caldera S, Pesce-Ares L. 2019b. In Vitro Transcription for
805 dgRNA v2. doi:10.17504/protocols.io.3bpgimn

806 Manning JE, Cantaert T. 2019. Time to Micromanage the Pathogen-Host-Vector Interface:
807 Considerations for Vaccine Development. *Nato Adv Sci Inst Se* 7:10.
808 doi:10.3390/vaccines7010010

809 Mi H, Muruganujan A, Huang X, Ebert D, Mills C, Guo X, Thomas PD. 2019. Protocol Update for
810 large-scale genome and gene function analysis with the PANTHER classification system
811 (v.14.0). *Nat Protoc* 14:703–721. doi:10.1038/s41596-019-0128-8

812 Ohnishi J, Piesman J, Silva AM de. 2001. Antigenic and genetic heterogeneity of Borrelia
813 burgdorferi populations transmitted by ticks. *Proceedings of the National Academy of*
814 *Sciences* 98:670–5. doi:10.1073/pnas.98.2.670

815 Ojaimi C, Mulay V, Liveris D, Iyer R, Schwartz I. 2005. Comparative Transcriptional Profiling of
816 Borrelia burgdorferi Clinical Isolates Differing in Capacities for Hematogenous Dissemination.
817 *Infect Immun* 73:6791–6802. doi:10.1128/iai.73.10.6791-6802.2005

818 Pal U, Kitsou C, Drecktrah D, Yaş OB, Fikrig E. 2022. Interactions Between Ticks and Lyme
819 Disease Spirochetes. *Curr Issues Mol Biol* 42:113–144. doi:10.21775/cimb.042.113

820 Pal U, Li X, Wang T, Montgomery RR, Ramamoorthi N, deSilva AM, Bao F, Yang X, Pypaert M,
821 Pradhan D, Kantor FS, Telford S, Anderson JF, Fikrig E. 2004. TROSPA, an Ixodes
822 scapularis Receptor for Borrelia burgdorferi. *Cell* 119:457–468.
823 doi:10.1016/j.cell.2004.10.027

824 Patro R, Duggal G, Love MI, Irizarry RA, Kingsford C. 2017. Salmon provides fast and bias-
825 aware quantification of transcript expression. *Nat Methods* 14:417 419.
826 doi:10.1038/nmeth.4197

827 Patton TG, Brandt KS, Nolder C, Clifton DR, Carroll JA, Gilmore RD. 2013. Borrelia burgdorferi
828 bba66 Gene Inactivation Results in Attenuated Mouse Infection by Tick Transmission. *Infect*
829 *Immun* 81:2488–2498. doi:10.1128/iai.00140-13

830 Phelan JP, Kern A, Ramsey ME, Lundt ME, Sharma B, Lin T, Gao L, Norris SJ, Hyde JA, Skare
831 JT, Hu LT. 2019. Genome-wide screen identifies novel genes required for Borrelia
832 burgdorferi survival in its Ixodes tick vector. *Plos Pathog* 15:e1007644.
833 doi:10.1371/journal.ppat.1007644

834 Radolf JD, Caimano MJ, Stevenson B, Hu LT. 2012. Of ticks, mice and men: understanding the
835 dual-host lifestyle of Lyme disease spirochaetes. *Nat Rev Microbiol* 10:87 99.
836 doi:10.1038/nrmicro2714

837 Rego ROM, Bestor A, Rosa PA. 2011. Defining the Plasmid-Borne Restriction-Modification
838 Systems of the Lyme Disease Spirochete Borrelia burgdorferi. *J Bacteriol* 193:1161–1171.
839 doi:10.1128/jb.01176-10

Rego ROM, Bestor A, Štefka J, Rosa PA. 2014. Population Bottlenecks during the Infectious Cycle of the Lyme Disease Spirochete Borrelia burgdorferi. *Plos One* 9:e101009. doi:10.1371/journal.pone.0101009

Revel AT, Talaat AM, Norgard MV. 2002. DNA microarray analysis of differential gene expression in Borrelia burgdorferi, the Lyme disease spirochete. *Proc National Acad Sci* 99:1562–1567. doi:10.1073/pnas.032667699

Ring K, Couper LI, Sapiro AL, Yarza F, Yang XF, Clay K, Mateusiak C, Chou S, Swei A. 2022. Host blood meal identity modifies vector gene expression and competency. *Mol Ecol* 31:2698–2711. doi:10.1111/mec.16413

Rosenberg R, Lindsey NP, Fischer M, Gregory CJ, Hinckley AF, Mead PS, Paz-Bailey G, Waterman SH, Drexler NA, Kersh GJ, Hooks H, Partridge SK, Visser SN, Beard CB, Petersen LR. 2018. Vital Signs: Trends in Reported Vectorborne Disease Cases — United States and Territories, 2004–2016. *Morbidity Mortal Wkly Rep* 67:496–501. doi:10.15585/mmwr.mm6717e1

Samuels DS, Lybecker MC, Yang XF, Ouyang Z, Bourret TJ, Boyle WK, Stevenson B, Drecktrah D, Caimano MJ. 2021. Gene Regulation and Transcriptomics. *Curr Issues Mol Biol* 42:223–266. doi:10.21775/cimb.042.223

Schneider CA, Rasband WS, Eliceiri KW. 2012. NIH Image to ImageJ: 25 years of image analysis. *Nat Methods* 9:671–675. doi:10.1038/nmeth.2089

Schwartz I, Margos G, Casjens SR, Qiu W-G, Eggers CH. 2021. Multipartite Genome of Lyme Disease Borrelia : Structure, Variation and Prophages. *Curr Issues Mol Biol* 42:409–454. doi:10.21775/cimb.042.409

Shaw WR, Catteruccia F. 2018. Vector biology meets disease control: using basic research to fight vector-borne diseases. *Nat Microbiol* 4:20–34. doi:10.1038/s41564-018-0214-7

Spielman A, Ribeiro JMC, Mather TN, Piesman J. 1987. Dissemination and Salivary Delivery of Lyme Disease Spirochetes in Vector Ticks (Acari: Ixodidae). *J Med Entomol* 24:201–205. doi:10.1093/jmedent/24.2.201

Steere AC, Sikand VK, Meurice F, Parenti DL, Fikrig E, Schoen RT, Nowakowski J, Schmid CH, Laukamp S, Buscarino C, Krause DS. 1998. Vaccination against Lyme Disease with Recombinant Borrelia burgdorferi Outer-Surface Lipoprotein A with Adjuvant. *New Engl J Medicine* 339:209–215. doi:10.1056/nejm199807233390401

Steere AC, Strle F, Wormser GP, Hu LT, Branda JA, Hovius JWR, Li X, Mead PS. 2016. Lyme borreliosis. *Nat Rev Dis Primers* 2:nrdp201690. doi:10.1038/nrdp.2016.90

Stevenson B, Zückert WR, Akins DR. 2000. Repetition, conservation, and variation: the multiple cp32 plasmids of Borrelia species. *J Mol Microb Biotech* 2:411–22.

875 Thomas PD, Ebert D, Muruganujan A, Mushayahama T, Albou L, Mi H. 2022. PANTHER:
876 Making genome-scale phylogenetics accessible to all. *Protein Sci* 31:8–22.
877 doi:10.1002/pro.4218

878 Tilly K, Rosa PA, Stewart PE. 2008. Biology of Infection with Borrelia burgdorferi. *Infect Dis Clin*
879 *N Am* 22:217 234. doi:10.1016/j.idc.2007.12.013

880 Tokarz R, Anderton JM, Katona LI, Benach JL. 2004. Combined Effects of Blood and
881 Temperature Shift on Borrelia burgdorferi Gene Expression as Determined by Whole
882 Genome DNA Array. *Infect Immun* 72:5419–5432. doi:10.1128/iai.72.9.5419-5432.2004

883 Zhang H, Marconi RT. 2005. Demonstration of Cotranscription and 1-Methyl-3-Nitroso-
884 Nitroguanidine Induction of a 30-Gene Operon of Borrelia burgdorferi: Evidence that the 32-
885 Kilobase Circular Plasmids Are Prophages. *J Bacteriol* 187:7985–7995.
886 doi:10.1128/jb.187.23.7985-7995.2005

887 Zhang L, Zhang Y, Adusumilli S, Liu L, Narasimhan S, Dai J, Zhao YO, Fikrig E. 2011.
888 Molecular Interactions that Enable Movement of the Lyme Disease Agent from the Tick Gut
889 into the Hemolymph. *Plos Pathog* 7:e1002079. doi:10.1371/journal.ppat.1002079

890 Zhu A, Ibrahim JG, Love MI. 2018. Heavy-tailed prior distributions for sequence count data:
891 removing the noise and preserving large differences. *Bioinformatics* 35:2084–2092.
892 doi:10.1093/bioinformatics/bty895

893